Modelling an angular accelerometer using frequency-response measurements

Jatiningrum, D; de Visser, CC; van Paassen, MM; Mulder, M

DOI
10.2514/6.2016-1139

Publication date
2016

Document Version
Accepted author manuscript

Published in
Proceedings of the AIAA guidance, navigation, and control conference

Modeling an Angular Accelerometer using Frequency-Response Measurements

D. Jatiningrum*, C. C. de Visser†, M. M. van Paassen‡, and M. Mulder§

Delft University of Technology, Delft, Zuid-Holland, 2629HS, The Netherlands.

A characterization of an angular accelerometer sensor is performed with a frequency-response experiment. To assess angular accelerometer dynamic properties, a position-based calibration table is utilized to provide the excitation input. The angular accelerometer specifications and calibration table limitations define a constrained test envelope for this particular setup. Measurement are obtained for a number of constant accelerations and varied with frequency. Analysis of the input-output relation in the frequency-domain leads to a frequency-response function model of the angular accelerometer. Time-domain data are used to validate the frequency-response model. A fourth-order structure is then preferred as the transfer-function for the 400 deg/s acceleration, with a 99.02 % fit. Besides representing the angular accelerometer dynamics, the angular accelerometer model is essential for the design of fault-tolerant flight control system.

Nomenclature

AA	Angular Accelerometer
CC	Control center
CT	Calibration Table
DAS	Data Acquisition System
FFT	Fast Fourier Transform
FPE	Akaike's Final Prediction Error
FRF	Frequency-Response Function
HR	Harmonics Ratio
IMU	Inertial Measurement Unit
MSE	Mean Squared Error
SNR	Signal-to-Noise Ratio
UUT	Unit Under Test

Symbols

α	AA measured angular acceleration, Volts
α_{est}	CT estimated angular acceleration, deg/s^2
θ	CT measured angular position, deg
θ_{est}	CT estimated angular position, deg
$a(s)$	System characteristic polynomial
$b(s)$	System polynomial

*PhD Student, Control and Simulation Section, Faculty of Aerospace Engineering, Delft University of Technology; Kluyverweg 1, 2629HS, Delft, The Netherlands, Member AIAA.

†Assistant Professor, Control and Simulation Section, Faculty of Aerospace Engineering, Delft University of Technology; Kluyverweg 1, 2629HS, Delft, The Netherlands, Member AIAA.

‡Associate Professor, Control and Simulation Section, Faculty of Aerospace Engineering, Delft University of Technology; Kluyverweg 1, 2629HS, Delft, The Netherlands.

§Professor, Control and Simulation Section, Faculty of Aerospace Engineering, Delft University of Technology; Kluyverweg 1, 2629HS, Delft, The Netherlands, Associate Fellow AIAA.

E	Prediction errors matrix
$e(t)$	Estimation signal
f	Frequency, Hz
F_s	Sampling rate, kHz
$G(s)$	Transfer Function
h	First six harmonics, dB
$h(t)$	System dynamics
h_f	Fundamental frequency, dB
M	Gain, dB
N	Total number of data, samples
n	Total number of sinusoids in one measurement range, cycles
n_p	Number of free parameters in the model
n_y	Number of output channels
Res_f	Frequency resolution, Hz
S/N	Signal-to-Noise Ratio, dB
T	Period of the sinusoid, s
U	Amplitude of the input signal, dB
$u(t)$	Input signal, deg/s^2
Y	Amplitude of the output signal, dB
$y(t)$	Output signal, V

I. Introduction

Design of the state-of-the art fault tolerant flight control system such as the Incremental Nonlinear Dynamic Inversion (INDI) technique[1] and Sensor-based Back-stepping (SBB) approach[2,3] can benefit from angular acceleration feedback. Such control systems can be made robust to model mismatch and have greatly increased performance compared to conventional nonlinear dynamic inversion. However, the feedback for these control laws is currently obtained by differentiating the rate gyro signals, which amplifies the inherent noise. A set of filters could be implemented to eliminate the noise; nevertheless a delay will be introduced. The performance of both control approaches are expected to be significantly improved when using angular accelerometers (AA) instead of differentiated gyro signals.

Although angular accelerometers are considered the key to increase the performance of several flight control approach, little is known regarding the relationship between the mechanical characteristics of the sensor and its performance. One of a study describes a development of an automated test system for angular accelerometer to assist the manufacturing and acceptance process.[4] Nonetheless, it concentrates on a research and development approach for an indirect angular acceleration sensor, which consists of a single-axis rate gyro, a gear and an electromagnetic inductorium.

When developing a flight control systems around this new AA, it is important to understand the frequency-response in the early stages of system design, since the AAs frequency-response will have a direct impact on the controller design and can help identify potential stability issues. Additionally, the angular accelerometer limitations and performance characteristics should also be recognized before designing the control system. Hence, a reliable sensor model is important in developing the novel concept of sensor-based flight control systems.

Thus far, the most direct approach for testing the frequency-response of an inertial sensor such as gyroscopes, is with an inertial rate table, or calibration table (CT), which is capable of introducing the appropriate frequency content.[5] This is because rate tables typically include a programmable servo motor and an optical encoder that verifies programmed rotation on the motor shaft. The advantage of this test approach is that it applies actual inertial motion with sensor-specific excitation.

Commonly known as turn-tables, CT are widely used to produce motion input with a single-axis, or multi degree-of-freedom two axis or three axis mounting platform. A CT is able to simulate aircraft attitude and orientation, with measurement applications not only for different types of inertial sensors, such as accelerometers and gyroscopes, but also to a group of sensors in for instance the Inertial Measurement Unit (IMU). Besides angular rate, typically this equipment also provides an estimated angular acceleration. However, the available CT accuracy is mainly intended for static operation.[6]

This study develops a suitable system identification technique to obtain the AA dynamic characteristics. In a case where the individual component values are not known, the frequency-response of the system, from input to output can be obtained experimentally and used to determine the transfer-function.[7] Frequency-response is a method where the frequency-dependent behaviour of a system is characterized by its response to sinusoidal signals.

The frequency-response method has been extensively studied, including the identification from experimental data approach[8,9] that is also used here. The concept of using a CT in a frequency-response based test is hypothetically applicable to AA as well. For this purpose, a CT is used to generate the motion input for the sensor. The input-output relationship analysed in frequency-domain is the primary observation, and validated with the time-domain data.[10] As a final point, the AA model is presented in a transfer-function form, which gives the functional relationship between physical input signal and electrical output signal.

The paper is divided into five sections, starting with an introduction to the topic. Section II contains background knowledge regarding the AA and CT system description. Section III describes the test envelope specification and measurement method for the frequency-response system identification. Section IV discusses the frequency-response analysis and transfer-function model development. Finally, Section V gives conclusive remarks on the AA model.

II. System Description

The following sub-sections introduce the sensor of interest and the experiment setup. Overview of the test system is presented in Figure 2.

A. Angular Accelerometer

The Unit Under Test (UUT) is a precision servo force balance AA, SR-207RFR, in Figure 1. This design is a pendulous type, makes use of the fluid rotor concept of sensing angular acceleration. It provides excellent bias stability and rejection of linear acceleration inputs[a]. The first fluid type inertia device can be traced back to 1940 as a device responsive to the rate of change of rotational speed, with an application in brake apparatus associated with the rotating element.[11] Whereas an angular classifying accelerometer with specific utility in its application to aircraft was developed in 1943.[12]

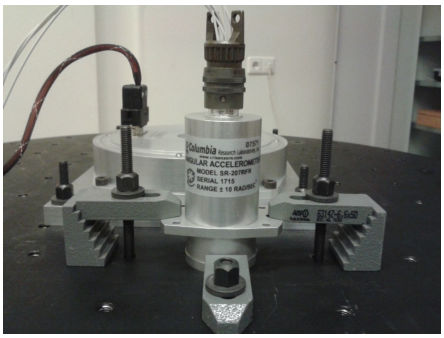

Figure 1. Angular accelerometer type SR-207RFR.

In initial experiments for this particular type of AA however, it appeared that the electrical noise produced when the sensor's signals were transmitted over the slip-rings of the measurement table exceeded the sensor's specifications. A slip ring is an electromechanical device that allows the transmission of power and electrical signals between a stationary to a rotating structure. In this case, the slip ring relays power to the sensor on the turn-table top, and sensor measurement signal to the Data Acquisition System (DAS). Adding a pre-sample filter in this basic setup did not lower the noise down to the required level, as compared to the direct connection of AA and DAS. Therefore, a customized setup was developed and discussed next.

B. Experiment Setup

A simplified schematic diagram of the customized measurement system is shown in Figure 2; its development has been addressed in a previous study.[13] Basically, an additional DAS was developed and placed on the turn-table, close to the sensor. The CT now consists of two parts: the control center (CC) and the two-axis turn-table. Besides hosting the control computer and CT DAS, the CC also accommodates a user interface from which measurement parameters such as motion mode, sampling frequency, recording options, and motion control can be regulated. The turn-table provides accurate angular position measurement and has unlimited angular freedom. The table's inner axis carries the rotating plate, on which the AA is mounted

[a]http://www.crlsensors.com, accessed on March, 2014

and secured. The AA sense the simulated inertial motion which is directly recorded in the sensor DAS, while the CT system only delivers power for the AA through the electrical access on the table top.

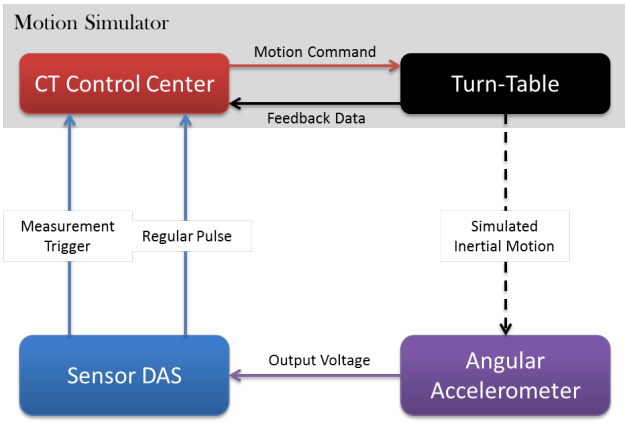

Figure 2. A simplified schematic diagram of the test measurement system.

The separate DAS consequently create two unsynchronized datasets one from the table and one from the AA, which means the logged data cannot be compared directly with each other. A feature of the CT is employed to assist the synchronization process: the freeze pulse. For this purpose, two signals are generated by sensor DAS computer and transmitted to the control center. The first is a trigger signal to start the recording process in both DAS. The second is a regular 100 Hz sync pulse that act as a common marker in synchronization. The concept is employed to align the sensor DAS computer and control center clocks, and furthermore the data.

The system of interest in this study is depicted in Figure 3. Since AA actually sense the CT angular acceleration, it is chosen as parameter input of the system. Even though the ideal system output is the AA raw data, the measured electrical signal has to be retrieved through a DAS and hence, introducing a measurement noise in the recorded data. Nevertheless, the sampled AA data is used as the system output.

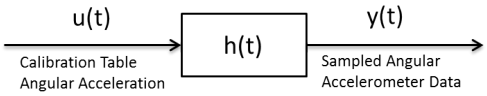

Figure 3. AA system block diagram.

III. Test Envelope and Method

For testing of a gyroscope, usually test are applied in which a constant rate of rotation is applied, with low or even zero acceleration.[14] However, this is not suitable for an AA which requires a varied angular velocity input. Therefore, the motion input should refer to angular acceleration, where the specifications are developed in the following sub-sections.

Here a sinusoidal acceleration profile is used to excite the sensor in the frequency range of interest. Typically, the input in frequency-response method is a frequency-sweep or broadband input,[15] where the sine frequency is modulated in one run. Nevertheless, single-frequency sine is used instead to acquire a strong, clear component in each frequency point in this study. The frequency points consequently needs to be specified in a proper approach to ensure the validity of the data, as illustrated in the test matrix. Once the frequency-response is obtained from the steady-state output sinusoid amplitude and phase angle, the data are combined in a Bode plot. Subsequently, the transfer-function of the system can be estimated from the frequency-response function.

A. Test Envelope Specification

Choosing test points for the frequency-response measurement should take into account the limitations of all the subsystems involved. Adhering to these constraints, the first is for the operational safety reason of the CT. Exceeding the specified, maximum factory acceleration for example, not only can be dangerous for the user, but could also potentially break the equipment itself. The second reason is to concentrate on the corresponding AA operational envelope in relation with its application in the future aircraft flight control systems. The test envelope boundaries are defined both by the CT and AA specifications, and illustrated in Figure 4.

- CT Factory Setting as the Motion Limits

  The motion limitations in this experiment are determined based on the CT performance envelope of the inner-axis and sinusoidal motion input. The factory setting is employed to establish the maximum restriction. It gives an acceleration limit of 1000 deg/s^2, and a rate limit of 1200 deg/s. The minimum motion is specified solely by the sensor.

- AA Operational Range as the Input Limit

  The AA specification is used for completing the boundary. The AA has a customized range of 10 rad/s^2[b] or 572.958 deg/s^2. For the purpose of the test, the maximum angular acceleration limit is set to 80% of the AA range at the most, which is 458.366 deg/s^2, or simplified to 450 deg/s^2. Then, the test envelope should include the minimum level that can be measured by the AA. Since the sensor lowest range is not specified in the data sheet, the noise level is used instead. The AA output noise level should be $\leq 3\ mV$, therefore, the value of 3 mV will serve as the minimum threshold of the input. To include the minimum threshold into the test envelope presented in Figure 4, the noise level should be converted from volts. Using the factory scale factor of 0.23 $V/rad/s^2$[c], results in 0.013 rad/s^2 or 0.747 deg/s^2 angular acceleration. To simplify, the level is rounded up to 0.8 deg/s^2.

- CT and AA Specifications to Determine the Bandwidth

  Another important limit is the bandwidth, a frequency range where measurement test points are established. Practically, the CT maximum bandwidth can range up to 30 Hz. Nevertheless, the actual terminal frequency, $f_{terminal}$, is highly dependent to the CT acceleration limit and excitation amplitude, as expressed in Equation 1.

$$f_{terminal}(rad) < \sqrt{\frac{AccelerationLimit}{ExcitationAmplitude}} \tag{1}$$

  The excitation amplitude is input related and therefore, is also determined by the sensor bandwidth.

  According to a previous sine-sweep measurement, the AA is able to measure up to frequencies around $8 - 9\ Hz$. Therefore, the highest test frequency is chosen to be at 8 Hz which translates to an amplitude of approximately 0.2 deg. With the CT axis 1 acceleration limit is 1000 deg/s^2 and the excitation amplitude chosen as 0.2 deg, $f_{terminal} = 70.711\ rad$. Equation 2 converts the terminal frequency to Hz.

$$f_{terminal}(Hz) < \frac{f_{terminal}(rad)}{2\pi} \tag{2}$$

  Then the terminal frequency should be less than 11.254 Hz. This value applies to the systems without payload. In this case, the terminal frequency is consequently reduced to 10 Hz, considering the new sensor DAS arrangement on top of the mounting plate.

  The minimum input line crosses the 0.2 deg amplitude line at approximately 0.33 Hz, as shown in Figure 4. The minimum frequency threshold is therefore set at 0.4 Hz.

B. Test Method

The experiment constitutes two groups of tests: constant-position and constant-acceleration. The constant-position test is bounded by a constant-amplitude sinusoidal input, varying frequency and acceleration. This group of measurements conducted at the 0.2 deg amplitude to accommodate the entire frequency range. The constant-acceleration test on the other hand, has four sub-groups that represent different accelerations at 1 deg/s^2, 10 deg/s^2, 100 deg/s^2 and 400 deg/s^2. Each of the four is varied in frequency and amplitude of the sinusoidal input. The constant position test points is represented by the green line in Figure 4, whereas blue lines are representing constant-acceleration test.

[b] AA Specification, http://www.crlsensors.com/
[c] AA Specification, http://www.crlsensors.com/

In order to examine the system dynamics, the test bandwidth is extended beyond the sensor maximum of 8 Hz to the table maximum bandwidth of 10 Hz. The starting point is the minimum frequency threshold at 0.4 Hz. Subsequent test points are in the increment of 20% from the previous value, up to 10 Hz. Additionally, round frequencies point of $1, 2, 3, 4, 5, 6, 7, 8$ and 9 Hz are included, which then gives a total of 28 frequency points.

The following list provides all the variables of interest recorded during the measurement, and estimated variables based on the measured data.

- θ (deg), CT measured angular position.
- θ_{est} (deg), CT estimated angular position.
- α_{est} (deg/s^2), CT estimated angular acceleration.
- α (V), AA measured angular acceleration.

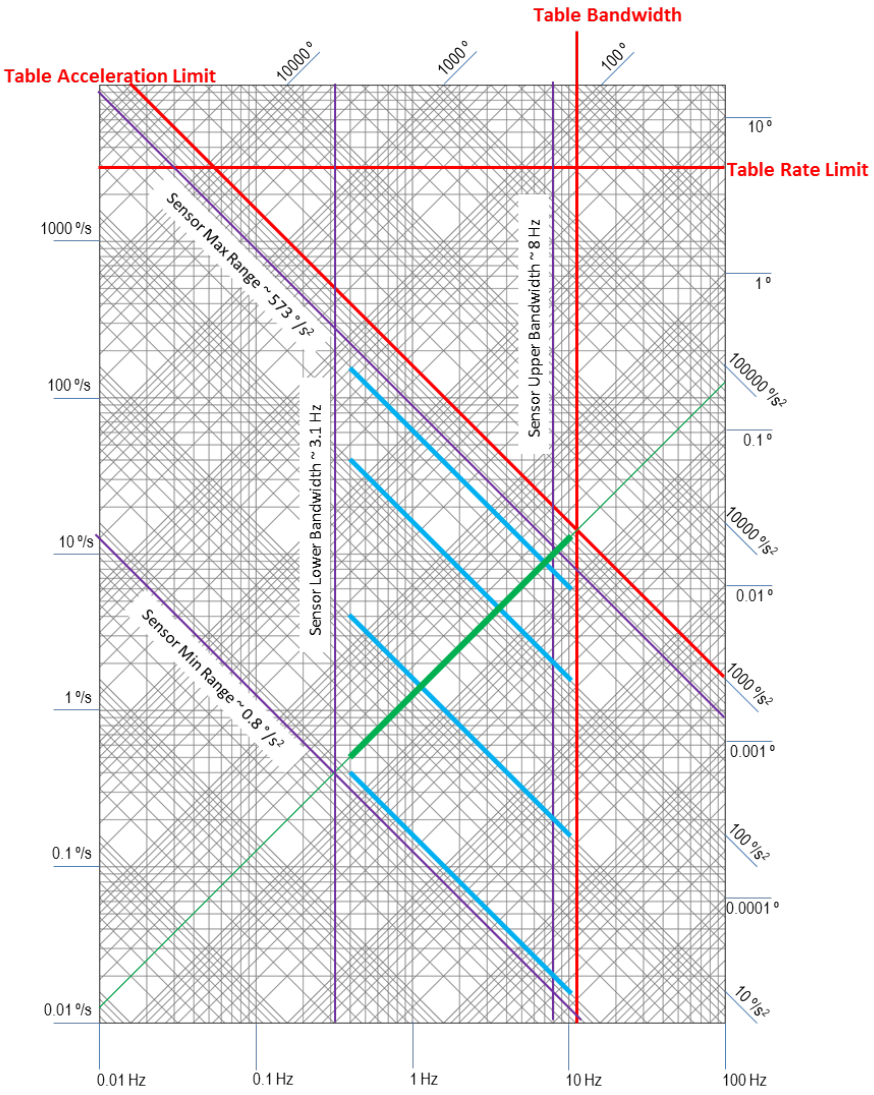

Figure 4. Frequency-response test envelope for the test axis. Test points of the constant position measurement are represented with the green line, while blue lines represent the constant acceleration test points.

The required measurement time is at least 100 s, with the data point needed for the FFT calculation in the power of 2. Using the calibration table maximum sampling rate of 2 kHz, it will result in 200,000 data points for a 100 s time span. Thus, the nearest power of 2 is 2^{18} or 262,144. Unfortunately, the CT computer could only accommodate up to 230,000 data points given the number of current recorded variables. Lowering the sampling rate is not preferable in favour of data synchronization. It was found that the synchronization has a 0.5 ms uncertainty for a lower sampling of 1 kHz. Therefore, the maximum sampling rate, F_s, of 2 kHz will still be used. A lower, nearest power of two number, 2^{17} or 131,072 data points was chosen instead. The measurement time itself is then adjusted accordingly to 65.536 s.

C. Test Matrix Development

In Section B, the test frequency points are defined as the increment of 20% from the previous value, starting from 0.4 Hz up to 10 Hz, and including the round frequency points. Furthermore, data size and measurement time were also prescribed to form a good base for the FFT calculation. However, with the sinusoid being

not fitting an integer number of complete cycles in the measurement period, leakage will present in the FFT spectrum. To correct the leakage, the chosen frequency points should be modified as such that each accommodates full cycles of sinusoid.

The sinusoid frequency adjustment calculation is shown in Table 1. The first column lists the frequency number. The second column presents the original frequencies. The required total number of data points, N, defined as 2^{17} or $131,072$, which results in a measurement time of $65.536\ s$ at $2\ kHz$ sampling rate. Frequency resolution at the chosen total samples is calculated with the following formula.

$$Res_f = \frac{F_s}{N} = \frac{2000}{131,072} = 0.01527\ Hz \tag{3}$$

An integer number of cycles was chosen in the third column for each original frequency, with the aim to create a new frequency as close as possible to the original but still contain an integer number of cycles, as listed in the fourth column. To inspect whether the new frequencies meet the requirement, the new period was calculated using the relation $T = 1/f_{new}$. The new period value, when multiplied with the new cycle, should result as the required measurement time, $65.536\ s$.

Table 1. New frequency estimation

Frequency (#)	Original Frequency (Hz)	N (cycles)	New Frequency (Hz)
1	0.4	26	0.396728516
2	0.48	31	0.473022461
3	0.576	38	0.579833984
4	0.6912	45	0.686645508
5	0.82944	54	0.823974609
6	0.995328	65	0.991821289
7	1	66	1.007080078
8	1.1943936	78	1.190185547
9	1.43327232	94	1.434326172
10	1.719926784	112	1.708984375
11	2	131	1.998901367
12	2.063912141	135	2.059936523
13	2.476694569	163	2.487182617
14	2.972033483	195	2.975463867
15	3	197	3.005981445
16	3.566440179	234	3.570556641
17	4	262	3.997802734
18	4.279728215	280	4.272460938
19	5	328	5.004882813
20	5.135673858	337	5.142211914
21	6	393	5.996704102
22	6.16280863	404	6.164550781
23	7	459	7.00378418
24	7.395370356	485	7.400512695
25	8	524	7.995605469
26	8.874444427	582	8.880615234
27	9	590	9.002685547
28	10	655	9.994506836

The new frequency points in Table 1 are used for the constant position measurement. In this measurement, the sine input has a constant amplitude and is varied in frequency. This way, the angular acceleration increases quadratically with frequency. In addition, several measurement points are exceeding the AA range, as can be seen by the green line in Figure 4. Therefore, it is better to use a constant acceleration test where the measurement can be maintained in the AA operating range. For a constant-acceleration test, the input should be specified by signal amplitude and frequency for each acceleration as presented in Table 2.

IV. Frequency-Response Analysis

The input-output relationship of the system is represented by two sets of data obtained from the frequency-response measurement. The CT angular acceleration represents the input of the system, and the AA measured angular acceleration represents the system output. Firstly, the data sets for each fre-

Table 2. Constant acceleration test points

Frequency (#)	Original Frequency (Hz)	New Frequency (Hz)	400 (deg/s^2)	100 (deg/s^2)	10 (deg/s^2)	1 (deg/s^2)
			Input Sinusoidal Amplitude (deg)			
1	0.4	0.396728516	64.374433330	16.093608333	1.609360833	0.160936083
2	0.48	0.473022461	45.283160252	11.320790063	1.132079006	0.113207901
3	0.576	0.579833984	30.136507666	7.534126917	0.753412692	0.075341269
4	0.6912	0.686645508	21.489934316	5.372483579	0.537248358	0.053724836
5	0.82944	0.823974609	14.923565519	3.730891380	0.373089138	0.037308914
6	0.995328	0.991821289	10.299909354	2.574977338	0.257497734	0.025749773
7	1	1.007080078	9.990155423	2.497538856	0.249753886	0.024975389
8	1.1943936	1.190185547	7.152714827	1.788178707	0.178817871	0.017881787
9	1.43327232	1.434326172	4.924979290	1.231244822	0.123124482	0.012312448
10	1.719926784	1.708984375	3.469157925	0.867289481	0.086728948	0.008672895
11	2	1.998901367	2.535814756	0.633953689	0.063395369	0.006339537
12	2.063912141	2.059936523	2.387770482	0.596942620	0.059694262	0.005969426
13	2.476694569	2.487182617	1.637890663	0.409472666	0.040947267	0.004094727
14	2.972033483	2.975463867	1.144434373	0.286108593	0.028610859	0.002861086
15	3	3.005981445	1.121315082	0.280328771	0.028032877	0.002803288
16	3.566440179	3.570556641	0.794746092	0.198686523	0.019868652	0.001986865
17	4	3.997802734	0.633953689	0.158488422	0.015848842	0.001584884
18	4.279728215	4.272460938	0.555065268	0.138766317	0.013876632	0.001387663
19	5	5.004882813	0.404494321	0.101123580	0.010112358	0.001011236
20	5.135673858	5.142211914	0.383177778	0.095794444	0.009579444	0.000957944
21	6	5.996704102	0.281757195	0.070439299	0.007043930	0.000704393
22	6.16280863	6.164550781	0.266622862	0.066655715	0.006665572	0.000666557
23	7	7.003784180	0.206554540	0.051638635	0.005163863	0.000516386
24	7.395370356	7.400512695	0.185002092	0.046250523	0.004625052	0.000462505
25	8	7.995605469	0.158488422	0.039622106	0.003962211	0.000396221
26	8.874444427	8.880615234	0.128473675	0.032118419	0.003211842	0.000321184
27	9	9.002685547	0.125013263	0.031253316	0.003125332	0.000312533
28	10	9.994506836	0.101432590	0.025358148	0.002535815	0.000253581

quency points are aligned using the freeze-pulse synchronization.[13] The data are then transformed to the frequency-domain using a Fast Fourier Transform (FFT).

The AA-CT setup is analysed as a single-input/ single-output system. The mathematical representation of the input signal is:

$$u(t) = U \sin 2\pi f t \tag{4}$$

where U is the amplitude of the input signal. The initial conditions are such that there is no transient response, or the transient response can be assumed to have decayed away to zero. This condition is achieved by initially running the turn-table for some time, then start the recording. The steady-state response in the output variable is represented by:

$$y_s(t) = Y(f) \sin(2\pi f t + \phi(f)) = UM(f) \sin(2\pi f t + \phi(f)) \tag{5}$$

Here M is the (amplitude) gain, and ϕ is the phase lag as a function of frequency. When the system is assumed linear, time-invariant, the frequency of $y_s(t)$ will be the same as in $u(t)$.

A. Signal-to-Noise and Harmonics Ratio

Due to the specific problem in this study, the frequency-domain representation of the signal is first examined. The characteristic is expressed in signal-to-noise (SNR) *power* ratio, which defined as:

$$S/N = \frac{\bar{s}^2(t)}{\bar{n}^2(t)} = \frac{signal\ power}{noise\ power} \tag{6}$$

The signal-to-noise ratio is commonly expressed in decibels. Thus:

$$S/N|_{dB} = 10\ log_{10} \frac{signal\ power}{noise\ power} \tag{7}$$

The signal power in SNR is generally characterized from the first six harmonics of the signal, whereas the noise power is the level of the background noise. A comparison of taking into account these first six

harmonics (6h) and only the fundamental frequency (1h) is presented in Figure 5. The SNR for the AA signal is shown in Figure 5(a), and Figure 5(b) display the SNR of the CT. The figures show the AA and CT SNR in constant acceleration measurement, for each acceleration point. For the AA, distortion appears at higher frequencies except for the 1 deg/s^2 acceleration. Whereas in CT case, the two lowest acceleration of 1 deg/s^2 and 10 deg/s^2 display no SNR distortion between the six harmonics and the fundamental harmonic calculation.

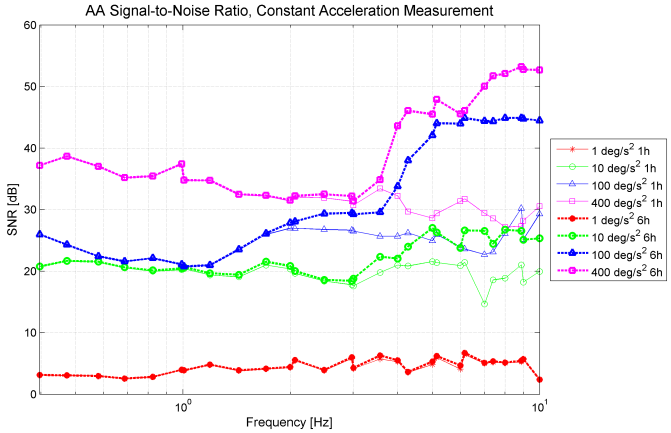

(a) AA.

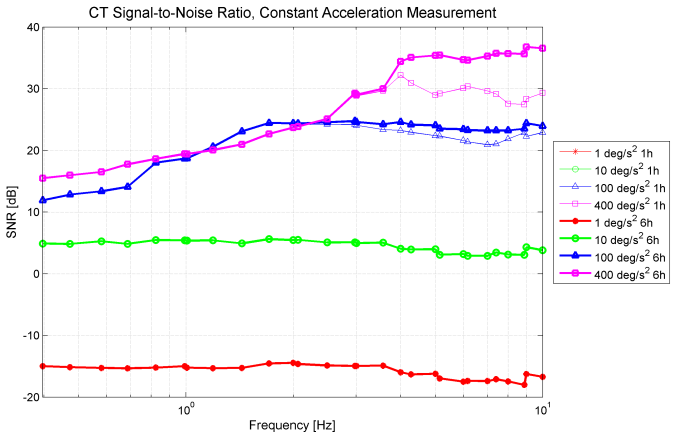

(b) CT.

Figure 5. AA and CT SNR of the constant acceleration measurement.

The harmonics ratio is defined as:

$$HR = \frac{\sum h}{h_f} \tag{8}$$

with h is the first six harmonics, and h_f is the fundamental frequency.

Taking the ratio between the next five harmonics and the fundamental frequency spectrum gives Figure 6(a) and Figure 6(b). Both figures show that the additional harmonics are increasing with frequency and acceleration. In each acceleration at the higher frequency, AA has higher harmonics ratio in comparison with CT. The higher ratio implies that the AA output is not entirely similar with the motion input, but the sensor dynamics also affect the measured angular acceleration. Thus, for higher frequencies, nonlinearities are present with a noticeably higher level in the AA.

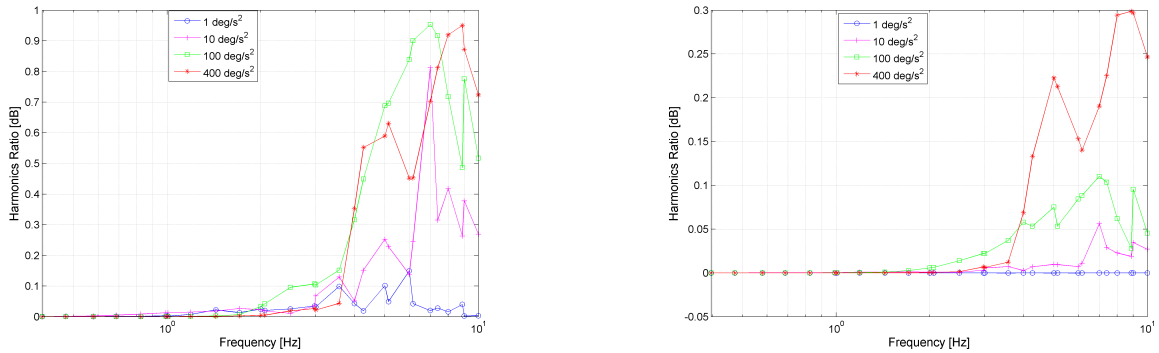

(a) AA. (b) CT.

Figure 6. AA and CT harmonics ratio of the constant acceleration measurement.

B. Gain Magnitude and Phase

The magnitude of the input-output relationship of the system is equal to the gain in (5), calculated as:

$$M(f) = \frac{Y(f)}{U} \tag{9}$$

f is frequency in Hz. Converting to decibel:

$$M|_{dB} = 20 * log_{10} M(f) \tag{10}$$

The phase frequency-response is given by:

$$\angle M(f) = \phi(f)_{out} - \phi(f)_{in} \tag{11}$$

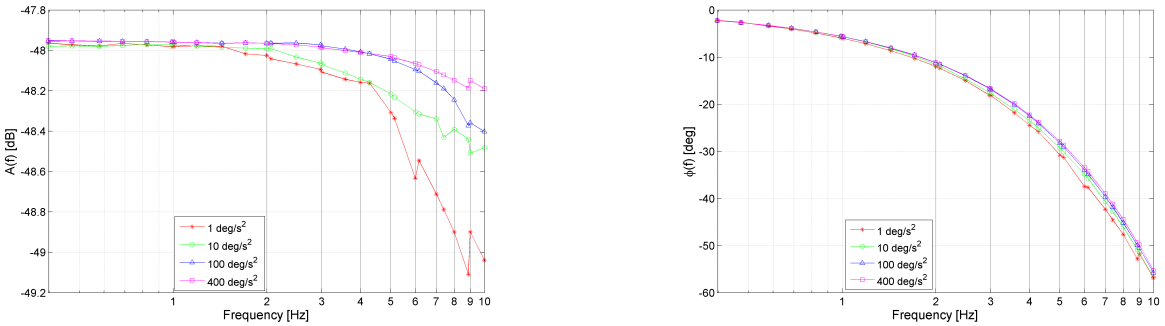

(a) Magnitude. (b) Phase.

Figure 7. Magnitude and phase of constant acceleration series frequency-response measurement with table angular acceleration as the reference.

Figure 7(a) shows the frequency-response function (FRF) result based on constant acceleration measurement with the table angular acceleration as the input/ reference. For this study, only the fundamental harmonics are taken into account. The magnitude appears flat at lower frequencies for all accelerations, where the two highest accelerations maintain the ratio up to 4 Hz and only decline at around 0.2 dB and 0.4 dB at the highest measured frequencies. The two lowest accelerations starts to decrease at around 2 Hz, with final values of 0.5 dB and 1 dB lower than at the initial frequencies. Due to the limitation of the CT as well as the current setup, the measurement bandwidth is limited to 10 Hz.

The phase response of the system is given in Figure 7(b). All responses are decreasing exponentially. The figure demonstrates that the phase responses are similar, indicating that they are not influenced by different accelerations, but only frequency-dependant.

For every frequency component, the phase response $\phi(f)$, gives the phase delay, defined as:

$$P(f) \cong -\frac{\phi(f)}{f} \tag{12}$$

Figure 8 present the phase delay $P(f)$ for constant acceleration measurement, which in this case gives the time delay in seconds experienced by each sinusoidal component of the input signal. At high accelerations of 100 deg/s^2 and 400 deg/s^2, the phase delay resembles a transport delay, where it has the same time delay for all frequencies or phase shift that is linear with frequency. However, the low acceleration of 10 deg/s^2 and especially 1 deg/s^2 have larger variations, which indicates there are probably influence from the non-linear system dynamics.

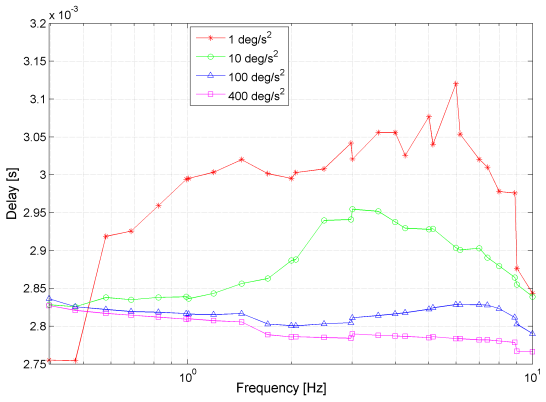

Figure 8. Phase delay of the constant acceleration phase response.

V. Angular Accelerometer Model Estimation using Time-Domain Data

Consider a linear system with the rational transfer-function, which can be represented by a ratio of polynomials:

$$G(s) = \frac{b(s)}{a(s)} \tag{13}$$

where $b(s)$ is the system polynomial and $a(s)$ is system characteristic polynomial. The transfer-function model is applied to the time domain data to relate the input and output. For illustration purpose, the evaluation is performed with a data set from 400 deg/s^2 acceleration.

The estimation is conducted using an ARX method, with model quality criteria outlined in Equation 14 to Equation 17.[d] The first measure of the result is Mean Squared Error (MSE), defined as:

$$MSE = \frac{1}{N}\sum_{t=1}^{N} e^T(t)e(t) \tag{14}$$

where $e(t)$ is the signal whose norm is minimized for estimation. Then, the second criteria is Akaike's Final Prediction Error (FPE), defined as:

$$FPE = \det(\frac{1}{N}E^T E)(\frac{1+\frac{n_p}{N}}{1-\frac{n_p}{N}}) \tag{15}$$

where n_p is the number of free parameters in the model; E is the N-by-n_y matrix of prediction errors, where n_y is the number of output channels. A raw measure of Akaike's Information Criterion as the third evaluator is defined as:

$$AIC = N\log(\det(\frac{1}{N}E^T E)) + 2 * n_p(n_y * \log(2\pi) + 1) \tag{16}$$

The last norm is Normalized Root Mean Squared Error (NRMSE) expressed as a percentage, which is defined as:

$$\text{FitPercent} = 100\left(1 - \frac{\| * y_{measured} - y_{model}\|}{\| * y_{measured} - \overline{y_{measured}}\|}\right) \tag{17}$$

For the first iteration, the model orders in the characteristic polynomial are chosen starting from 0^{th} to 5^{th} order, which also represent the number of poles. These initial models are numbered from one to six

[d] http://nl.mathworks.com/help/ident/ug/model-quality-metrics.html, accessed on November, 2015

in Table 3, and each coupled with the same number of zero. Based on the quality criteria, the best fit is obtained from the 4^{th} order or model number 5. Overall, it has the lowest error estimate and AIC. Therefore, the fifth order model is selected as the initial estimate.

Table 3. Time-domain data estimation model quality criteria

Model	Order	MSError	FPE	AIC	Fit (%)
1	0^{th}	0.137	0.252	-1.378	60.92
2	1^{st}	2.506×10^{-5}	0.0038	-5.561	94.98
3	2^{nd}	2.474×10^{-6}	0.0038	-5.568	95
4	3^{rd}	9.622×10^{-8}	2.987×10^{-4}	-8.116	98.49
5	$\mathbf{4^{th}}$	$\mathbf{1.992 \times 10^{-8}}$	$\mathbf{1.274 \times 10^{-4}}$	$\mathbf{-8.969}$	**99.02**
6	5^{th}	2.067×10^{-8}	1.296×10^{-4}	-8.951	99.01
7	$4^{th}, 1zero$	1.72×10^{-7}	3.426×10^{-4}	-7.979	98.43
8	$4^{th}, 2zero$	2.762×10^{-8}	1.519×10^{-4}	-7.792	98.93
9	$4^{th}, 3zero$	2.569×10^{-8}	1.484×10^{-4}	-8.816	98.94

The iteration is further continued by varying the number of zeros in the initial transfer-function, or model number 5. These estimations are represented by models number 7 to 9, with each 1, 2 and 3 zeros. Results show that none of the extended models yields a better estimate compared to the initial model. None of the models yield lower criterion values, their fits are all lower than model 5. Additionally, the model should represent the same order of input and output since the same variables, angular acceleration from CT and AA, were used to built the frequency-response representation. For those reasons, model 5 is settled as the preferred transfer-function with the following structure.

$$G(s) = \frac{-1.672 \times 10^{-4} s^4 - 0.028 s^3 - 68.74 s^2 + 2.164 \times 10^4 s + 188.7}{s^4 + 314.4 s^3 + 6.589 \times 10^4 s^2 + 5.408 \times 10^6 s + 4.426 \times 10^4} \tag{18}$$

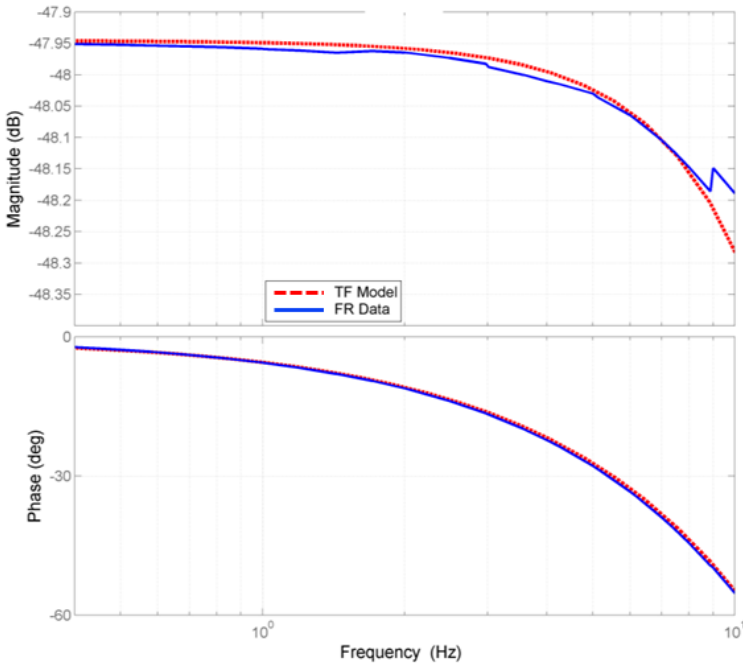

Figure 9. Frequency-response of the fourth-order transfer-function model output and FRF.

Comparison between model and measurement frequency-response and phase are presented in Figure 9. Frequency-response of the fifth-order transfer-function model output in Equation 18 is depicted in dashed, red line. Meanwhile, the blue line display frequency-response of 400 deg/s^2 acceleration measurement spectral data from Figure 7(a). Observing the plot, one could mention that the frequency-response measurement did not demonstrate the full sensor dynamics. At the terminal frequency of 10 Hz, the magnitude plot has not shown the -3 dB roll off per decade. Comparably, the phase plot ends shortly before -60 deg instead of the -360 deg range.

Unfortunately, measurement for higher frequencies are not possible due to the system setup limitation. The transfer-function model of course, could predict the response for wider bandwidth as shown in Figure 10, thus demonstrate the approximation of the full system dynamics. The red box highlight the area of the frequency-response measurement result. Based on the magnitude plot, the system bandwidth progress up to about 25 Hz before it declines. The expected linearity of the input-output pair of CT and AA angular accelerations is evident in this system bandwidth.

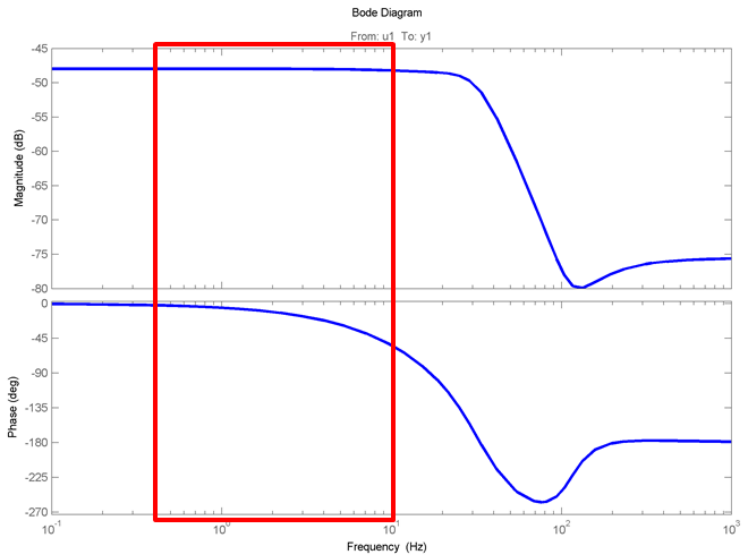

Figure 10. Bode plot of the fourth-order transfer-function model.

Nonetheless, an alternative approach could be performed by taking advantage of the additional spectral component which appears at twice the fundamental frequency in constant rate motion. Future work will evaluate the possibility to utilize this component in order to extend the frequency-response range, and finally to have an enhanced AA model.

VI. Conclusion

An angular accelerometer and a calibration table were measured with the goal of obtaining the frequency-response of the system for the transfer-function model estimation. With the analysis conducted in the frequency-domain, the test points were specified as such to reduce variance and prevent leakage in the spectral estimate. The boundary condition of the test was determined based on the AA specification and CT limitation, manifested in a test envelope of the experiment setup and a test matrix for the selected frequency points.

The input-output relation in the frequency domain results in the frequency-response of the system for every acceleration values. To validate the estimated transfer-function, a model was generated using the time-domain form of the data. Transfer function with ARX method in several model structures are employed to approximate the relation of CT angular acceleration as the input and AA data as the output. It was observed that a fourth-order transfer-function gives the finest approximation of the system, with a 99.02 % fit and lowest criterion content.

For the specified bandwidth and acceleration, a transfer-function model was developed in this study. This model is expected to facilitate the development of the novel fault-tolerant, flight control system by providing a model of accurate angular acceleration feedback information.

References

[1]Sieberling, S., Chu, Q. P., and Mulder, J. A., "Robust Flight Control Using Incremental Nonlinear Dynamic Inversion and Angular Acceleration Prediction," *Journal of Guidance, Control, and Dynamics*, Vol. 33, No. 6, 2010, pp. 1732–1742.

[2]Falkena, W., Borst, C., van Oort, E. R., and Chu, Q. P., "Sensor-Based Backstepping," *Journal of Guidance, Control, and Dynamics*, Vol. 36, No. 2, 2013, pp. 606–610.

[3]Sun, L. G., de Visser, C. C., Chu, Q. P., and Falkena, W., "Hybrid Sensor-Based Backstepping Control Approach with Its Application to Fault-Tolerant Flight Control," *Journal of Guidance, Control, and Dynamics*, Vol. 37, No. 1, 2014, pp. 59–71.

[4]Pan, S. and Wang, B., "An Automatic Test System for Angular Accelerometer," *Proceedings of the Seventh International Symposium on Instrumentation and Control Technology: Measurement Theory and Systems and Aeronautical Equipment*, SPIE, 2008, p. 7.

[5]Looney, M., "Analyzing Frequency Response of Inertial MEMS in Stabilization Systems," Electronic Article, www.analog.com/analogdialogue, 2012.

[6]Anon., "IEEE Standard Specification Format Guide and Test Procedure for Non-gyroscopic Inertial Angular Sensors Jerk, Acceleration, Velocity, and Displacement," Std 671^{TM}-1985 (r2008), IEEE, 1985.

[7]Nise, N. S., *Control Systems Engineering*, John Wiley and Sons, Inc., 2011.

[8]Shieh, L. S. and Cohen, M. H., "Transfer Function Fitting from Experimental Frequency-Response Data," *Journal of Computers and Electrical Engineering*, Vol. 5, No. 3, 1978, pp. 205–212.

[9]Hurle, D., Joyce, G., and Wilson, G., "A Technique for Experimentally Determining the Transfer Function of a Czochralski Pulling Process," *Journal of Crystal Growth*, Vol. 74, 1986, pp. 480–490.

[10]Ljung, L., "Some Results on Identifying Linear Systems Using Frequency Domain Data," *Proceedings of the 32nd Conference on Decision and Control*, IEEE, San Antonio, Texas, USA, 1993, pp. 3534–3538.

[11]Sexton, E. P., Patent, United States Patent Office, Dec. 1940.

[12]Buchanan, J. A., Patent, United States Patent Office, Feb. 1943.

[13]Jatiningrum, D., Muis, A., de Visser, C. C., van Paassen, M. M., and Mulder, M., "A High-Precision Position Turn-Table as the Reference for Angular Accelerometer Calibration Experiment," *Proceedings of the 5th CEAS Air and Space Conference*, CEAS, Delft, The Netherlands, 2015.

[14]Kirkko-Jaakkola, M., Collin, J., and Takala, J., "Bias Prediction for MEMS Gyroscopes," *IEEE Sensors Journal*, Vol. 12, 2012, pp. 2157–2163.

[15]Tischler, M. B. and Remple, R. K., *Aircraft and Rotorcraft System Identification*, American Institute of Aeronautics and Astronautics, Inc., 2012.